

KINETIC ALFVÉN TURBULENCE BELOW AND ABOVE ION-CYCLOTRON FREQUENCY

J. S. ZHAO^{1,2}, Y. M. VOITENKO³, D. J. WU¹ AND M. Y. YU^{4,5}

¹ Purple Mountain Observatory, Chinese Academy of Sciences, Nanjing 210008, China. js_zhao@pmo.ac.cn

² Key Laboratory of Solar activity, National Astronomical Observatories, Chinese Academy of Sciences, Beijing 100012, China.

³ Solar-Terrestrial Centre of Excellence, Space Physics Division, Belgian Institute for Space Aeronomy, Ringlaan-3-Avenue Circulaire, B-1180 Brussels, Belgium

⁴ Institute for Fusion Theory and Simulation and Department of Physics, Zhejiang University, Hangzhou 310027, China. and

⁵ Institute for Theoretical Physics I, Ruhr University, D-44780 Bochum, Germany

Draft version August 27, 2021

ABSTRACT

Alfvénic turbulent cascade perpendicular and parallel to the background magnetic field is studied accounting for anisotropic dispersive effects and turbulent intermittency. The perpendicular dispersion and intermittency make the perpendicular-wavenumber magnetic spectra steeper and speed up production of high ion-cyclotron frequencies by the turbulent cascade. On the contrary, the parallel dispersion makes the spectra flatter and decelerate the frequency cascade above the ion-cyclotron frequency. Competition of the above factors results in spectral indices distributed in the interval [-2,-3], where -2 is the index of high-frequency space-filling turbulence, and -3 is the index of low-frequency intermittent turbulence formed by tube-like fluctuations. Spectra of fully intermittent turbulence fill a narrower range of spectral indices [-7/3,-3], which almost coincides with the range of indexes measured in the solar wind. This suggests that the kinetic-scale turbulent spectra are shaped mainly by dispersion and intermittency. A small mismatch with measured indexes of about 0.1 can be associated with damping effects not studied here.

Subject headings: MHD and kinetic Alfvén waves – turbulence – solar corona – solar wind

1. INTRODUCTION

Alfvénic turbulence, measured in situ by satellites in the Earth’s space environment (Chaston et al. 2008, 2009; Huang et al. 2012, 2014) and in the solar wind (Sahraoui et al. 2010; He et al. 2011, 2013; Alexandrova et al. 2012; Horbury et al. 2012; Salem et al. 2012; Podesta 2013; Roberts et al. 2013, 2015), extends from magnetohydrodynamic (MHD) scales down to ion and even electron kinetic scales. Turbulence at kinetic scales is often referred to as kinetic Alfvén turbulence. Theoretical models have shown that kinetic Alfvén turbulence is generated naturally through an anisotropic Alfvén wave cascade produced by interactions among counterstreaming Alfvén wave packets (e.g., Kraichnan 1965; Goldreich & Sridhar 1995; Quataert & Gruzinov 1999; Cranmer & van Ballegoijen 2003; Schekochihin et al. 2009; Bian et al. 2010; Howes et al. 2011b; Zhao et al. 2013). Transition of Alfvénic turbulence from MHD to kinetic scales depends strongly on the plasma thermal to magnetic pressure ratio (β). For example, the low-frequency turbulent cascade first arrives to the ion gyroradius scale in $\beta > Q$ plasmas and to the electron inertial scale in $\beta < Q$ plasmas, where $Q = m_e/m_i$ is the electron to ion mass ratio (e.g., Zhao et al. 2013).

When the cascade reaches kinetic scales, the Kolomogorov-like spectrum $k_{\perp}^{-5/3}$ of perpendicular magnetic and electric fluctuations transforms into the steeper $k_{\perp}^{-7/3}$ for the magnetic spectrum and the flatter $k_{\perp}^{-1/3}$ for the electric spectrum (e.g., Schekochihin et al. 2009). The anisotropic scaling $k_z \propto k_{\perp}^{2/3}$ at MHD scales becomes $k_z \propto k_{\perp}^{1/3}$ (for $\beta > Q$) and $k_z \propto k_{\perp}^{7/3}$ (for $\beta < Q$) at kinetic scales (Zhao et al. 2013), where k_z and k_{\perp} are the wavenumbers parallel and perpendicular to the

background magnetic field \mathbf{B}_0 . Therefore, with the increasing k_{\perp} the parallel wavenumber k_z and the Alfvén wave frequency ω ($\sim V_A k_z$) are also increasing, where V_A is the Alfvén speed. When the parallel wave scale approaches the ion inertial length λ_i , the Alfvén wave frequency approaches the ion-cyclotron frequency ω_{ci} , $\omega/\omega_{ci} \sim \lambda_i k_z \sim 1$. At this point the low-frequency $\omega < \omega_{ci}$ kinetic Alfvén turbulence transforms into the high-frequency $\omega \gtrsim \omega_{ci}$ kinetic Alfvén (sometimes named “quasi-perpendicular whistler”) turbulence. Observations support the idea that high-frequency Alfvén waves can be generated by low-frequency Alfvén waves via turbulent cascade (Huang et al. 2012). Linear theories also agree that the kinetic Alfvén branch can extend from low- to high-frequency domain (Sahraoui et al. 2012; Vásconez et al. 2014; Zhao et al. 2014b).

It is not yet certain what effects make observed turbulent spectra $\propto k_{\perp}^{-2.8}$ (Alexandrova et al. 2012; Sahraoui et al. 2013) steeper than the regular turbulent spectrum of KAWs $\propto k_{\perp}^{-7/3}$ (see Schekochihin et al. 2009, and references therein). Two feasible mechanisms discussed recently are Landau damping (Howes et al. 2011) and intermittency (Boldyrev & Perez 2012). If the turbulent cascade generates high-frequency KAW, the spectra can be modified by dispersive effects of finite $\lambda_i k_z$. High-frequency KAWs undergo also ion-cyclotron wave-particle interactions (e.g., Voitenko & Goossens 2002), which can contribute to the turbulent spectra in addition to Landau damping. Kinetic damping leads to the plasma heating and particles acceleration both along and across $B_0 \parallel z$, connecting particles to waves in the solar-terrestrial environments (Marsch 2006). High-frequency effects in Alfvénic turbulence are understood much less than the low-frequency ones.

Here we use a two-fluid plasma model to investigate dispersive effects (in particular, of finite $\omega/\omega_{ci} \sim \lambda_i k_z$) and intermittency in Alfvénic turbulence and explore the wavenumber and frequency spectra from MHD to kinetic scales. Influence of damping on the turbulent spectra is not taken into account, which restricts applicability of our results to the cases where spectral modifications due to damping are weak in comparison to the modifications due to dispersion and intermittency. In Discussion we argue this is often the case in the solar wind.

In the next Section we introduce a model for anisotropic Alfvénic turbulence and corresponding wavenumber spectra. The steady spectra in the frequency space are presented in Section 3. Effects introduced by the turbulent intermittency are described in Section 4. Section 5 presents the spectral distributions in solar flare loops and in solar wind at 1 AU. Section 6 discusses impacts of the injection scales, intermittency and dissipative effects. The last section presents a summary of obtained results. In Appendix A the analytical expressions of the wave variables and their spectral distributions are derived for low- β plasmas, and in Appendix B the analytical results are extended to the case of intermittent turbulence.

2. ANISOTROPIC ALFVÉNIC TURBULENCE

The steady-state spectral properties of Alfvénic turbulence can be investigated phenomenologically using a model developed by (e.g., Schekochihin et al. 2009), where turbulence is stirred initially through collisions of counterstreaming Alfvén wave-packets at the (spatial and temporal) MHD scales. In the collisions, the local wave-wave interaction condition as well as the critical balance condition are assumed to be satisfied. The latter corresponds to strong Alfvénic turbulence where the nonlinear timescale becomes as short as the linear timescale.

To obtain the steady-state spectrum, one makes use of linear responses of the Alfvén mode, namely the quasi-linear premise (Schekochihin et al. 2009; Howes et al. 2011a; Zhao et al. 2013). Therefore, for the spectrum of the high-frequency kinetic-scale Alfvénic turbulence, one needs the linear relations for high-frequency kinetic Alfvén wave (KAW). Recently, Zhao et al. (2014b) derived the linear KAW responses at parallel length-scales extending down to the ion inertial length and below, with corresponding frequencies extending to $\omega \sim \omega_{ci}$ and above. Below we use these results to obtain the high-frequency Alfvénic turbulent spectra and scalings.

In the case of local nonlinear interactions, the spectral energy flux can be written as (Zhao et al. 2013),

$$\epsilon = C_1^{-3/2} k_\perp \delta v_{e\perp} \delta b_\perp^2, \quad (1)$$

where C_1 is of order unity, $\delta v_{e\perp}$ is the perpendicular electron velocity fluctuation, and δb_\perp is the perpendicular magnetic fluctuation in velocity units, $\delta b_\perp \equiv V_A \delta B_\perp / B_0$. Using the relation

$$\delta v_{e\perp} = \bar{\omega} \mathcal{L} \delta b_\perp,$$

we get

$$\delta b_\perp = C_1^{1/2} \epsilon^{1/3} \bar{\omega}^{-1/3} k_\perp^{-1/3} \mathcal{L}^{-1/3}, \quad (2)$$

where the normalized frequency of oblique Alfvén waves

is (Zhao et al. 2014b)

$$\bar{\omega} \equiv \left[\frac{\mathcal{R} + 2\beta}{2(\mathcal{L}' + \mathcal{L}^2\beta)} \left(1 + \sqrt{1 - 4\beta \frac{\mathcal{L}' + \mathcal{L}^2\beta}{(\mathcal{R} + 2\beta)^2}} \right) \right]^{1/2}, \quad (3)$$

with the definitions $\beta = k_B (T_i + T_e) / (m_i V_A^2)$, $\mathcal{R} \equiv 1 + \rho^2 k_\perp^2$, $\mathcal{L} \equiv 1 + \lambda_e^2 k_\perp^2$, $\mathcal{L}' \equiv 1 + \lambda_e^2 k_\perp^2 + \lambda_i^2 k_z^2$, $\rho = \sqrt{k_B (T_i + T_e) / m_i} / \omega_{ci}$, $\lambda_i = V_A / \omega_{ci}$, and $\lambda_e = \sqrt{m_e / m_i} \lambda_i$. The Alfvén wave dispersion $\omega = V_A k_z \bar{\omega}$ is valid at the quasi-perpendicular propagations, $k_\perp^2 / k_z^2 \gg 1$, in the MHD and kinetic ranges without restrictions on ω / ω_{ci} .

From the critical balance condition that the linear Alfvén time is equal to the nonlinear turnover time (Goldreich & Sridhar 1995),

$$\omega^{-1} = (C_2 \delta v_{e\perp} k_\perp)^{-1},$$

we present the anisotropy scaling relation as

$$k_z = C_1^{1/2} C_2 V_A^{-1} \epsilon^{1/3} \bar{\omega}^{-1/3} k_\perp^{2/3} \mathcal{L}^{2/3}, \quad (4)$$

where C_2 is a constant of order unity. Note since the magnetic field is frozen into the electron before the turbulence cascading into electron gyroradius scale, the electron velocity $\delta v_{e\perp}$ is used to estimate the nonlinear turnover time.

Linear relations between electric and magnetic fluctuations are given by

$$\delta e_\perp = \bar{\omega} \Gamma \delta b_\perp$$

and

$$\delta e_z = \bar{\omega} (\Gamma - 1) (k_z / k_\perp) \delta b_\perp,$$

where $\delta e_\perp \equiv \delta E_\perp / B_0$ and $\delta e_z \equiv \delta E_z / B_0$. Together with Equations (2) and (4) one can then obtain the scaling relations for the electric components:

$$\delta e_\perp = C_1^{1/2} \epsilon^{1/3} k_\perp^{-1/3} \bar{\omega}^{2/3} \mathcal{L}^{-1/3} \Gamma, \quad (5)$$

and

$$\delta e_z = C_1 C_2 V_A^{-1} \epsilon^{2/3} k_\perp^{-2/3} \bar{\omega}^{-1/3} \mathcal{L}^{1/3} (\Gamma - 1), \quad (6)$$

where $\Gamma \equiv \mathcal{L} \tilde{T}_i + (1/\bar{\omega}^2 - \lambda_i^2 k_z^2) \tilde{T}_e$ and $\tilde{T}_{e,i} \equiv T_{e,i} / (T_e + T_i)$. The parallel electric field δe_z in Equation (6) is usually much smaller than the perpendicular electric field δe_\perp in Equation (5), but δe_z can play an important role in the particles energization along \mathbf{B}_0 .

From Equations (2) and (5) we obtain the following magnetic and electric power spectra:

$$\begin{aligned} P_{\delta b_\perp} &= k_\perp^{-1} \delta b_\perp^2 \\ &= C_1 \epsilon^{2/3} \bar{\omega}^{-1/3} k_\perp^{-5/3} \mathcal{L}^{-1/3}, \end{aligned} \quad (7)$$

$$\begin{aligned} P_{\delta e_\perp} &= k_\perp^{-1} \delta e_\perp^2 \\ &= C_1 \epsilon^{2/3} \bar{\omega}^{4/3} k_\perp^{-5/3} \mathcal{L}^{-2/3} \Gamma^2. \end{aligned} \quad (8)$$

The physical quantities and spectra (2)–(8) reduce to their MHD counterparts when the kinetic factors ρk_\perp , $\lambda_e k_\perp$ and $\lambda_i k_z$ vanish. In low- β ($\beta \ll 1$) plasmas, expressions (2)–(8) can be simplified (see in Appendix A).

Note that the turbulence scalings in plasmas $\beta \sim 1$ is nearly the same as that in $Q \ll \beta \ll 1$ due to the similar properties of KAWs in these plasma environments.

Properties of the spectral scalings and physical quantities are summarized in Table 1 for three β regimes: inertial ($\beta \ll Q$), transition ($\beta \sim Q$), and kinetic ($Q \ll \beta < 1$). Electron and ion temperatures are assumed to be equal, $T_i = T_e$, so that $\rho \simeq 1.4\rho_i \simeq 1.4\rho_s$, where $\rho_i = \sqrt{k_B T_i / m_i / \omega_{ci}}$ is the ion gyroradius, and $\rho_s = \sqrt{k_B T_e / m_e / \omega_{ce}}$ is the ion-acoustic gyroradius.

At MHD scales, where all ρk_\perp , $\lambda_e k_\perp$, and $\lambda_i k_z$ are small, the scalings shown in Table 1 are consistent with those described by (Goldreich & Sridhar 1995) for the strong MHD Alfvénic turbulence. As the turbulence cascades into the kinetic scales, there can be two cases: (i) for the large perpendicular kinetic effect $\lambda_e k_\perp > \lambda_i k_z$ in the inertial and transition regimes, and $\rho k_\perp > 1$ and $\lambda_i k_z \lesssim 1$ in the kinetic regime (outside the parenthesis), and (ii) for the large parallel kinetic effect $\lambda_i k_z > \lambda_e k_\perp$ in the inertial and transition regimes, and $\lambda_i k_z > \rho k_\perp$ in the kinetic regime (inside the parenthesis). In the latter case, the wave frequency is larger than the ion cyclotron frequency, and two limits $\lambda_e k_\perp < \lambda_i k_z \ll (Q/\beta)^{1/2}$ and $\lambda_i k_z \gg \max(\lambda_e k_\perp, (Q/\beta)^{1/2})$ are used to consider two different effects in contributing the parallel electric field δe_z in Eq. (A3). We see that $k_z \propto k_\perp^{7/3}$ (k_\perp^3) in the inertial regime where $\lambda_e k_\perp \gg 1 \gg \rho k_\perp$, and $k_z \propto k_\perp^2$ ($k_\perp^{5/2}$) in the transition regime where $\lambda_e k_\perp \sim \rho k_\perp \gg 1$, which means the turbulence cascade proceeds mainly towards the \mathbf{B}_0 direction. We found several new scalings, i.e., $P_{\delta b_\perp} \propto k_\perp^{-1}$ in the inertial regime and $P_{\delta b_\perp} \propto k_\perp^{-2}$ in the kinetic regime. We also note that the scalings in the inertial regime at $\rho k_\perp \gg 1$, as well as in the kinetic regime at $\lambda_e k_\perp \gg 1$, are the same as that in the transition regime.

3. FREQUENCY SPECTRA

Accounting for the anisotropy relation (4), we can write the scaling of the wave frequency as

$$\omega = C_1^{1/2} C_2 \epsilon^{1/3} \bar{\omega}^{2/3} k_\perp^{2/3} \mathcal{L}^{2/3}, \quad (9)$$

whose asymptotic forms in low- β plasmas are given in Table 1. The power spectra $P_{\delta b_\perp}(\omega)$ and $P_{\delta e_\perp}(\omega)$ are found from the energy balance condition $k_\perp P_{\delta b_\perp, e_\perp}(k_\perp) = \omega P_{\delta b_\perp, e_\perp}(\omega)$, which also presented in Table 1. Note that in the inertial regime the wave frequency approaches ω_{ci} as $\lambda_i k_z > \lambda_e k_\perp > 1$. It shows that the universal spectrum $P_{\delta b_\perp}(\omega) \propto \omega^{-2}$ arises in all ranges, whereas $P_{\delta e_\perp}(\omega)$ varies in different limits. The universal frequency spectrum of magnetic power is not a surprising result, it is rather a direct consequence of the constant energy flux and critical balance that we assume here.

4. IMPACT OF INTERMITTENCY ON TURBULENT SPECTRA AND PRODUCTION OF HIGH FREQUENCIES

Our previous analysis assumed a space-filling turbulence where the turbulent fluctuations of any particular scale cover all the volume occupied by the turbulence. However, Alfvénic turbulence observed in solar-terrestrial plasmas often exhibits a non space-filling, i.e. intermittent character (e.g., Chaston et al. 2008; Huang et al. 2012; Wu et al. 2013; Chen et al. 2014). Recent

PIC simulations also suggest a non space-filling Alfvénic turbulence at kinetic scales (Wu et al. 2013). Two-fluid simulations by Boldyrev & Perez (2012) and gyrokinetic simulations by TenBarge & Howes (2013) explored the intermittent KAW turbulence extending from ion to electron scale. The spectral index $\sim -8/3$ obtained by Boldyrev & Perez (2012) is similar to the spectrum -2.8 obtained by TenBarge & Howes (2013) (also see Howes et al. 2011). Both above studies suggest that intermittency affects the spectral scalings in kinetic Alfvénic turbulence.

Here, we further assume that the Alfvénic turbulence is mostly space-filling at the MHD scales but becomes intermittent at kinetic scales. Adopting the same approach as was used by Boldyrev & Perez (2012), in Appendix B we obtain analytical expressions and steady-state spectra for different kinds of the intermittent Alfvénic turbulence. The corresponding turbulence scalings are presented in Table 2, where two kinds of intermittent structures are considered, sheet-like ($\alpha = 1$) and tube-like ($\alpha = 2$). The normalized wavenumbers are ordered as $\lambda_e k_\perp \gg 1 \gg \rho k_\perp$ in the very low- β plasmas ($\beta < Q$); $\lambda_e k_\perp \sim \rho k_\perp \gg 1$ for the transition $\beta \sim Q$; and $\rho k_\perp \gg 1 \gg \lambda_e k_\perp$ for $\beta > Q$.

The perpendicular wavenumber spectrum ($\tilde{P}_{\delta b_\perp}$ in Table 2) is steeper in the intermittent turbulence than in the space-filling turbulence ($P_{\delta b_\perp}$ in Table 1), such that $\tilde{P}_{\delta b_\perp} = k_\perp^{-\alpha/3} P_{\delta b_\perp}$. The same concerns also electric spectra, $\tilde{P}_{\delta e_\perp} = k_\perp^{-\alpha/3} P_{\delta e_\perp}$. As α varies between 1 and 2 depending on the fractional content of the sheet- and tube-like intermittent fluctuations, the magnetic spectral index spans the range $R_{\text{int}} = [-7/3, -3]$ in the wavenumber range $\rho_i k_\perp > 1$ and $\lambda_i k_z \lesssim 1$ at $Q \ll \beta \ll 1$. We believe that the spectra are the same also in $\beta \sim 1$ plasmas where KAW properties are similar to that at $Q \ll \beta \ll 1$. Such β values are typical for the solar wind at 1AU.

It is interesting to note that the parallel wavenumber k_z and frequency ω spectra of the intermittent turbulence (Table 2) are also steeper than the corresponding spectra of the space-filling turbulence (Table 1). It means that the parallel turbulence scale and wave frequency in the intermittent turbulence approaches the ion inertial length λ_i and ion cyclotron frequency ω_{ci} faster than in the space-filling turbulence. In other words, turbulent intermittency facilitates generation of high-frequency KAWs by the turbulent cascade. Table 2 also shows that the magnetic frequency spectrum retains its original form $\propto \omega^{-2}$, while the electric frequency spectrum varies depending on the β/Q ratio.

Recently, Sahraoui et al. (2013) have analyzed magnetic spectra selected from 10 years of Cluster observations. This analysis has shown that the spectral index at scales between ion and electron gyroradii is distributed in the range $[-2.5, -3.1]$ with a peak at about -2.8 . This range is almost the same as the range R_{int} predicted for the intermittent turbulence, which suggests that the kinetic-scale solar wind turbulence is intermittent. A slight (about 0.1) down-shift of the measured range as compared to R_{int} may be caused by the dissipative effects that are not taken into account in the present study.

5. TWO EXAMPLES

TABLE 1
TURBULENCE SCALINGS. SCALINGS ABOVE THE ION-CYCLOTRON FREQUENCY ARE SHOWN IN PARENTHESIS.

Parameter	Inertial regime ($\beta \ll Q$)		Transition regime ($\beta \sim Q$)		Kinetic regime ($Q \ll \beta \ll 1$)	
	$1/k_{\perp} \gg \lambda_e$	$\lambda_e \gg 1/k_{\perp} \gg \rho$	$1/k_{\perp} \gg \lambda_e \sim \rho$	$\lambda_e \sim \rho \gg 1/k_{\perp}$	$1/k_{\perp} \gg \rho$	$\rho \gg 1/k_{\perp} \gg \lambda_e$
$P_{\delta b_{\perp}}(k_{\perp})$	$k_{\perp}^{-5/3}$	$k_{\perp}^{-7/3}(k_{\perp}^{-1})$	$k_{\perp}^{-5/3}$	$k_{\perp}^{-3}(k_{\perp}^{-2})$	$k_{\perp}^{-5/3}$	$k_{\perp}^{-7/3}(k_{\perp}^{-2})$
$P_{\delta e_{\perp}}(k_{\perp})$	$k_{\perp}^{-5/3}$	$k_{\perp}^{-1/3}(k_{\perp}^{-3a}, k_{\perp}^{9b})$	$k_{\perp}^{-5/3}$	$k_{\perp}(k_{\perp}^5)$	$k_{\perp}^{-5/3}$	$k_{\perp}^{-1/3}(k_{\perp})$
$\delta e_z(k_{\perp})$	$k_{\perp}^{4/3}$	$k_{\perp}^{5/3}(k_{\perp}^a, k_{\perp}^7b)$	$k_{\perp}^{4/3}$	$k_{\perp}^2(k_{\perp}^{9/2})$	$k_{\perp}^{4/3}$	$k_{\perp}^{-1/3}(k_{\perp}^{1/2})$
$k_z(k_{\perp})$	$k_{\perp}^{2/3}$	$k_{\perp}^{7/3}(k_{\perp}^3)$	$k_{\perp}^{2/3}$	$k_{\perp}^2(k_{\perp}^{5/2})$	$k_{\perp}^{2/3}$	$k_{\perp}^{1/3}(k_{\perp}^{1/2})$
$\omega(k_{\perp})$	$k_{\perp}^{2/3}$	$k_{\perp}^{4/3}(\omega \rightarrow \omega_{ci})$	$k_{\perp}^{2/3}$	$k_{\perp}^2(k_{\perp})$	$k_{\perp}^{2/3}$	$k_{\perp}^{4/3}(k_{\perp})$
$P_{\delta b_{\perp}}(\omega)$	ω^{-2}	ω^{-2}	ω^{-2}	$\omega^{-2}(\omega^{-2})$	ω^{-2}	$\omega^{-2}(\omega^{-2})$
$P_{\delta e_{\perp}}(\omega)$	ω^{-2}	$\omega^{-1/2}$	ω^{-2}	$\omega^0(\omega^5)$	ω^{-2}	$\omega^{-1/2}(\omega)$

^a a for $\lambda_e k_{\perp} < \lambda_i k_z \ll (Q/\beta)^{1/2}$.

^b b for $\lambda_i k_z \gg \max(\lambda_e k_{\perp}, (Q/\beta)^{1/2})$.

TABLE 2
TURBULENCE SCALINGS FOR INTERMITTENT KINETIC ALFVÉN TURBULENCE. SCALINGS ABOVE THE ION-CYCLOTRON FREQUENCY ARE SHOWN IN PARENTHESIS.

Parameter	Inertial regime ($\beta \ll Q$)		Transition regime ($\beta \sim Q$)		Kinetic regime ($Q \ll \beta \ll 1$)	
	sheet-like	tube-like	sheet-like	tube-like	sheet-like	tube-like
$\tilde{P}_{\delta b_{\perp}}(k_{\perp})$	$k_{\perp}^{-8/3}(k_{\perp}^{-4/3})$	$k_{\perp}^{-3}(k_{\perp}^{-5/3})$	$k_{\perp}^{-10/3}(k_{\perp}^{-7/3})$	$k_{\perp}^{-11/3}(k_{\perp}^{-8/3})$	$k_{\perp}^{-8/3}(k_{\perp}^{-7/3})$	$k_{\perp}^{-3}(k_{\perp}^{-8/3})$
$\tilde{P}_{\delta e_{\perp}}(k_{\perp})$	$k_{\perp}^{-2/3}(k_{\perp}^{-10/3a}, k_{\perp}^{26/3b})$	$k_{\perp}^{-1}(k_{\perp}^{-11/3a}, k_{\perp}^{25/3b})$	$k_{\perp}^{2/3}(k_{\perp}^{14/3})$	$k_{\perp}^{1/3}(k_{\perp}^{13/3})$	$k_{\perp}^{-2/3}(k_{\perp}^{2/3})$	$k_{\perp}^{-1}(k_{\perp}^{1/3})$
$\delta \tilde{e}_z(k_{\perp})$	$k_{\perp}^{7/3}(k_{\perp}^{5/3a}, k_{\perp}^{23/3b})$	$k_{\perp}^3(k_{\perp}^{7/3a}, k_{\perp}^{25/3b})$	$k_{\perp}^{8/3}(k_{\perp}^{31/6})$	$k_{\perp}^{10/3}(k_{\perp}^{35/6})$	$k_{\perp}^{1/3}(k_{\perp}^{7/6})$	$k_{\perp}^1(k_{\perp}^{11/6})$
$\tilde{k}_z(k_{\perp})$	$k_{\perp}^{8/3}(k_{\perp}^{10/3})$	$k_{\perp}^3(k_{\perp}^{11/3})$	$k_{\perp}^{7/3}(k_{\perp}^{17/6})$	$k_{\perp}^{8/3}(k_{\perp}^{19/6})$	$k_{\perp}^{2/3}(k_{\perp}^{5/6})$	$k_{\perp}^1(k_{\perp}^{7/6})$
$\tilde{\omega}(k_{\perp})$	$k_{\perp}^{5/3}(k_{\perp}^{1/3})$	$k_{\perp}^2(k_{\perp}^{2/3})$	$k_{\perp}^{7/3}(k_{\perp}^{4/3})$	$k_{\perp}^{8/3}(k_{\perp}^{5/3})$	$k_{\perp}^{5/3}(k_{\perp}^{4/3})$	$k_{\perp}^2(k_{\perp}^{5/3})$
$\tilde{P}_{\delta b_{\perp}}(\omega)$	$\omega^{-2}(\omega^{-2})$	$\omega^{-2}(\omega^{-2})$	$\omega^{-2}(\omega^{-2})$	$\omega^{-2}(\omega^{-2})$	$\omega^{-2}(\omega^{-2})$	$\omega^{-2}(\omega^{-2})$
$\tilde{P}_{\delta e_{\perp}}(\omega)$	$\omega^{-4/5}(\omega^{-8a}, \omega^{28b})$	$\omega^{-1}(\omega^{-5a}, \omega^{13b})$	$\omega^{-2/7}(\omega^{13/4})$	$\omega^{-1/2}(\omega^{11/5})$	$\omega^{-4/5}(\omega^{1/4})$	$\omega^{-1}(\omega^{-1/5})$

^a a for $\lambda_e k_{\perp} < \lambda_i k_z \ll (Q/\beta)^{1/2}$.

^b b for $\lambda_i k_z \gg \max(\lambda_e k_{\perp}, (Q/\beta)^{1/2})$.

5.1. Solar flare loops

Large nonthermal broadening of spectral lines, observed in the solar flares, has been supposed to be produced by the plasma turbulence (e.g., Alexander et al. 1998 and references therein). Let us consider excitation of the Alfvénic turbulence in a solar flare loop with the length $L_{0z} = 5 \times 10^6$ m, width $L_{0\perp} = 10^4$ m, internal magnetic field $B_0 \simeq 5 \times 10^{-2}$ T, number density $n_0 \simeq 10^{15} \text{ m}^{-3}$, and temperature $T_i = T_e \simeq 10^6$ K (Zhao et al. 2013). We have then $\beta \simeq 1.4 \times 10^{-5}$, and the KAWs are in the inertial β regime, $\beta < Q$. It is reasonable to assume that the initial fluctuations perturbing the loop have the scales that are close to the loop dimensions, $\lambda_{0\perp} \simeq L_{0\perp}$ and $\lambda_{0z} \simeq L_{0z}$, such that $k_{0z}/k_{0\perp} = 2 \times 10^{-3}$.

The deduced from spectral observations non-thermal velocities $V_{nt} = 100 - 200 \text{ km s}^{-1}$ (Alexander et al. 1998 and references therein) allow estimating the turbulence amplitude $\delta B_{0\perp}$ at the driving scale $k_{0\perp}$. Assuming that the turbulence is driven at MHD scales, and using the MHD turbulent spectrum $\sim k_{\perp}^{-5/3}$, the relation $V_{nt}^2 \simeq V_{turb}^2$ gives

$$\begin{aligned} \frac{V_{nt}^2}{V_A^2} &= \frac{\delta B_{turb}^2}{B_0^2} = \frac{\delta B_{0\perp}^2}{B_0^2} \int_{k_{0\perp}}^{k_d} \frac{dk_{\perp}}{k_{0\perp}} \left(\frac{k_{\perp}}{k_{0\perp}} \right)^{-5/3} \\ &= \frac{3}{2} \left(1 - \left(\frac{k_{d\perp}}{k_{0\perp}} \right)^{-2/3} \right) \frac{\delta B_{0\perp}^2}{B_0^2}, \quad (10) \end{aligned}$$

where the contribution originating from the dissipation scale $k_{d\perp}$ can be neglected for a wide inertial range $k_{d\perp}/k_{0\perp} \gg 1$. Then, taking for certainty $V_{nt} = 140 \text{ km s}^{-1}$, we estimate $\delta B_{0\perp}/B_0 \simeq 2 \times 10^{-3}$ and the perturbative approach is justified. In this case, the critical balance condition $k_{0z}/k_{0\perp} = \delta B_{0\perp}/B_0$ is satisfied already at the driving scales. The initial wave frequency $\omega \simeq 43 \text{ rad s}^{-1}$ is 5 orders below the ion cyclotron frequency $\omega_{ci} \simeq 5 \times 10^6 \text{ rad s}^{-1}$.

Based on the above parameters, Figure 1 presents spectral scaling for the turbulence in the flare loop. It is seen that the turbulent cascade arrives to the high ion cyclotron frequencies at the perpendicular scales that are already smaller than the ion gyroradius scale. Therefore, the scalings of the kinetic Alfvén turbulence are mainly defined by the perpendicular dispersive effects of finite $\lambda_e k_{\perp}$, which result in the magnetic spectrum $\propto k_{\perp}^{-7/3}$, electric spectrum $\propto k_{\perp}^{-1/3}$, anisotropic scale relation $k_z \propto k_{\perp}^{7/3}$, and frequency scaling $\omega \propto k_{\perp}^{4/3}$. It is interesting to observe the increase of the parallel electric field E_z as the wavelength decreases, which attains large values $E_z \sim 0.1 - 1 \text{ V/m}$ at kinetic scales. These values are larger than the Dreicer field $E_D = e \ln \Lambda / (4\pi \epsilon_0 \lambda_D^2) \sim 10^{-2} \text{ V/m}$, so that the turbulence-generated parallel electric fields may play an important role in the field-aligned particle acceleration and/or plasma heating in flare loops. One however should keep in mind that our results are valid only in the wavenumber ranges where

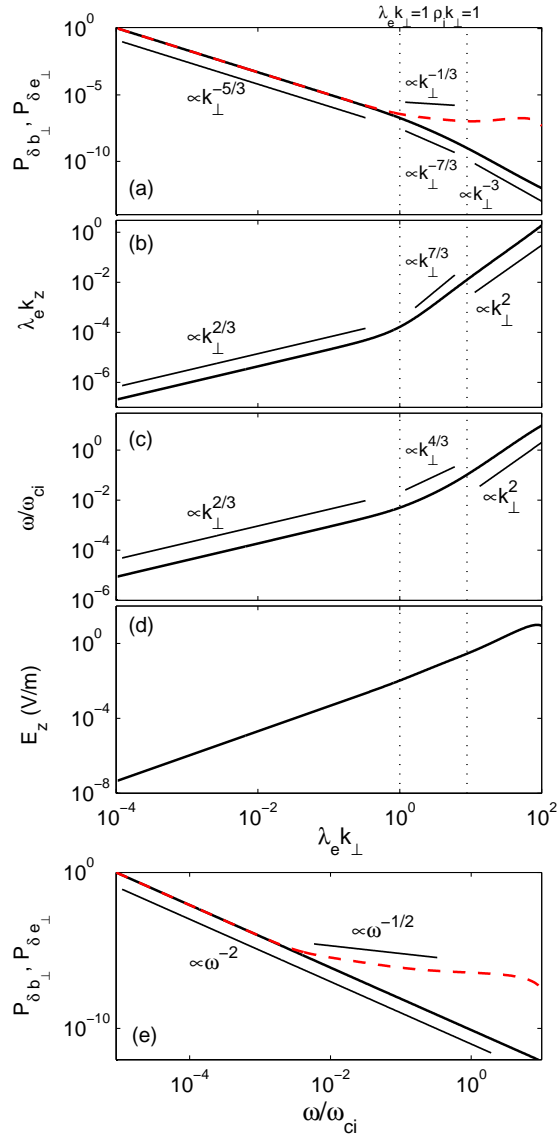


FIG. 1.— Steady-state spectral distributions in a typical flare loop plasma. (a) Normalized energy spectra for δb_{\perp} (solid line), and δe_{\perp} (dashed line). (b) The anisotropy relation. (c) The wave frequency versus the perpendicular wavenumber. (d) The parallel electric field versus the perpendicular wavenumber. (e) Normalized energy spectra of δb_{\perp} (solid line) and δe_{\perp} (dashed line) versus the wave frequency.

damping is relatively weak (see Discussion). At high wavenumbers one may need to account for dissipative effects (and for electron dispersive effects at $\rho_e k_{\perp} \geq 1$).

The parallel dispersive effects are not expected to be significant in the considered here case of the low-frequency driver perturbing the whole loop. However, Alfvénic perturbations excited by kinetic instabilities may be high-frequency from the very beginning (see e.g. Voitenko and Goossens 2002), in which case the parallel dispersive effects of finite $\lambda_i k_z$ must be taken into account. We also do not discuss here the intermittency effects because it is difficult to deduce from the available observations if the turbulence in flare loops is intermittent.

5.2. Solar wind at 1 AU

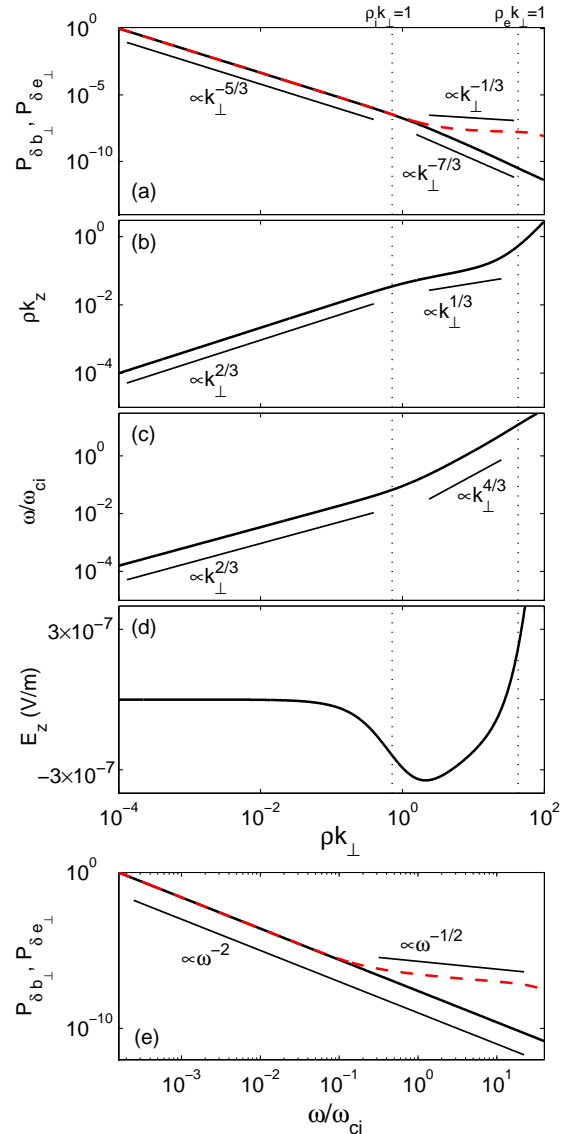


FIG. 2.— Steady-state Alfvén wave spectra in a typical solar wind plasma. (a) Normalized energy spectra for δb_{\perp} (solid line), and δe_{\perp} (dashed line). (b) The anisotropy relation. (c) The wave frequency versus the perpendicular wavenumber. (d) The parallel electric field versus the perpendicular wavenumber. (e) Normalized energy spectra of δb_{\perp} (solid line) and δe_{\perp} (dashed line) versus the wave frequency.

Typical plasmas parameters are $B_0 \simeq 11$ nT, $N_0 \simeq 9 \times 10^6$ m $^{-3}$, $T_i \simeq 1.5 \times 10^5$ K and $T_e \simeq 1.4 \times 10^5$ K in the solar wind at 1 AU (Salem et al. 2012). Here $\beta \sim 0.4$. We consider high-amplitude magnetic perturbations $\delta B_{0\perp} \sim B_0$, at the isotropic initial (injection) scales $L_{0z} = L_{0\perp} = 3 \times 10^9$ m, which imply that the critical balance is set up at the very beginning. The corresponding initial wave frequency $\omega \simeq 1.7 \times 10^{-4}$ rad s $^{-1}$ is much less as compared to the ion-cyclotron frequency $\omega_{ci} \simeq 1$ rad s $^{-1}$. Based on above parameters, the spectral scalings are presented in Figure 2.

From Figure 2 we see that the wave frequency reaches the ion cyclotron frequency well above the ion gyroradius scales. In this case kinetic effects of finite $\rho_e k_{\perp}$ dominate kinetic spectral scalings and result in the magnetic spectrum $\propto k_{\perp}^{-7/3}$, electric spectrum $\propto k_{\perp}^{-1/3}$, anisotropy

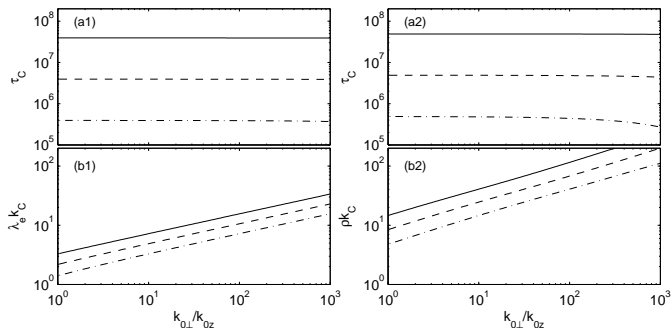


FIG. 3.— The spatial and temporal scales, τ_c and k_c , for different initial energy injection scale and anisotropy ratio. The solid, dashed, and dash-dotted lines represent $\lambda_i k_{0z} = 10^{-5}$, 10^{-4} and 10^{-3} , respectively. The plasma parameters used in panels (a1) and (b1) are the same as that in figure 1; the plasma parameters in panels (a2) and (b2) are the same as that in figure 2.

scale relation $k_z \propto k_\perp^{1/3}$, and frequency scaling $\omega \propto k_\perp^{4/3}$ in the range $\rho_i k_\perp > 1 > \rho_e k_\perp$. Although magnetic amplitudes are high at the injection scales, they drop well below B_0 as the turbulence cascades towards the small scales, such that $\delta B_\perp/B_0 \sim 0.05$ at the ion gyroradius scale $\rho_i k_\perp = 1$ and $\delta B_\perp/B_0 \sim 0.005$ at the electron gyroradius scale $\rho_e k_\perp = 1$. The sign “-” in front of E_z in Panel (d) represents the phase shift between E_z and δB_\perp .

However, the above scalings disagree with observed ones. Sahraoui et al. (2013) have found that magnetic spectra $\propto k_\perp^{-7/3}$ are unlikely in the kinetic-scale solar wind turbulence. Most of the observed kinetic-scale spectra are significantly steeper, with the spectral index distributed in the range $[-2.5, -3.1]$. The observed range of spectral indices is very close to that predicted in the previous section for the intermittent turbulence, $[-7/3, -3]$ (see also Table II). This suggests that the kinetic-scale turbulence in the solar wind is intermittent, with the steepest spectra dominated by the low-frequency tube-like fluctuations, whereas the flattest spectra indicate the presence of sheet-like structures and/or high frequencies. The intermittent character of the solar wind turbulence at kinetic scales has been supported by recent Cluster observations of magnetic (Wu et al. 2013) and density (Chen et al. 2014) fluctuations.

6. DISCUSSION

6.1. Impact of the injection scales on the excitation of high-frequency KAWs

To further understand the frequency cascade in Alfvénic turbulence, it is of interest to estimate the time required for the wave frequency to cascade from the initial driving frequency $\omega = \omega_0$ to the ion cyclotron frequency $\omega = \omega_{ci}$. Assume that the perpendicular wavenumber doubles at each (j -th) cascade step, $k_{\perp(j)} = 2k_{\perp(j-1)}$. The time of the j -th cascade step is $t_j = 2\pi/\omega(k_{\perp j})$. If after n cascades, at the critical wavenumber $k_{\perp c} = k_{\perp(n)}$ the wave frequency reaches ω_{ci} , the time required is $\tau \sim \sum_{j=1}^n 2\pi/\omega(k_{\perp j})$. Figure 3 shows the normalized time scale $\tau_c \equiv \tau/(2\pi/\omega_{ci}) = \sum_{j=1}^n (\omega_{ci}/\omega(k_{\perp j}))$ and the corresponding perpendicular wavenumber $k_{\perp c}$ as functions of the initial anisotropy $k_{0\perp}/k_{0z}$, for different injection scales $\lambda_i k_{0z}$. We see that the wave frequency can reach ω_{ci} in the vicinity of the

plasma kinetic scales. Figure 3 also shows that larger $\lambda_i k_{0z}$ and $k_{0z}/k_{0\perp}$ leads to shorter time τ_c and smaller wavenumber $k_{\perp c}$ at which the ion cyclotron frequency is reached. Thus, detailed comparison of our theoretical predictions with the satellite observations would require more definite information on $\lambda_i k_{0z}$ and $k_{0\perp}/k_{0z}$, which are not certain at present.

Earlier studies have shown that the ions of the solar atmosphere can be accelerated by Alfvén waves at the ion cyclotron frequency. It is therefore of interest to consider the generation of such Alfvén waves by the turbulent cascade. We consider a plasma in the solar active region (Gary 2001), where $B_0 = 10^{-3}$ T, $n = 10^{15}$ m $^{-3}$, and $T = 3 \times 10^6$ K, $\beta \simeq 0.1$ and $\omega_{ci} \simeq 10^5$ rad/s. The times for the turbulent cascade to generate Alfvén waves at the ion cyclotron frequency are $\tau \sim 0.1$ s, 1 s, and 10 s for $\lambda_i k_{0z} = 10^{-3}$, 10^{-4} and 10^{-5} , respectively. The corresponding spatial scales are $L \sim V_A \tau \sim 10^5$ m, 10^6 m, and 10^7 m, respectively. These scales are smaller than the global spatial scales $\sim 10^8 - 10^9$ m (temporal scales, tens minutes) of the active regions. Therefore, ion cyclotron Alfvén waves may be easily excited by the Alfvénic turbulence cascade in the solar active regions, where sources of the initial Alfvén waves can be convective motions of the magnetic foot-points, particle fluxes, and/or magnetic reconnection.

6.2. Impact of intermittency and spectra contamination by high frequencies

Recent results on solar wind turbulence reported by Sahraoui et al. (2013) indicate steep spectra at kinetic scales, with spectral indices distributed in the interval $[-2.5, -3.1]$. Such spectra can be formed by the intermittent Alfvénic turbulence, which is supported by the high intermittency measured in the solar wind turbulence at kinetic scales (Wu et al. 2013; Chen et al. 2014). Extending analysis below electron gyroradius scale, Alexandrova et al. (2012) proposed a complex spectral form $\propto k_\perp^{-8/3} \exp(-k_\perp \rho_e)$ which is nearly the power-law $\propto k_\perp^{-8/3}$ between the ion and electron gyroradius and mostly exponential below the electron gyroradius. The power-law part of the spectrum ($\propto k_\perp^{-8/3}$) may be formed by the intermittent turbulence with sheet-like structure (Boldyrev & Perez 2012), and steeper observed spectra can be formed by adding tube-like structures. The exponential spectrum drop at $k_\perp \rho_e > 1$ implies the appearance of the dissipation range, and may be caused by the strong electron Landau damping (TenBarge & Howes 2013). On the other hand, not exponential but steep power-law spectra below the electron gyroradius scale were reported by Sahraoui et al. (2010, 2013), who also suggested possible reasons for that. Further observations and analysis are needed to distinguish the nature of turbulence at scales below ρ_e and to resolve the mentioned above controversy. We did not study this range of scales.

Direct comparisons between spacecraft-frame frequency spectra and theoretical wavenumber spectra may be complicated by violation of the Taylor hypothesis. Namely, as we have shown above, the KAW frequency can increase to $\omega \gtrsim \omega_{ci}$, in which case the contribution of the term $\sim \omega$ to the spacecraft-frame frequency $\omega_{sc} = \omega + k \cdot v_{sw}$ may become as important as the contri-

bution of Doppler term $\sim k \cdot v_{sw}$. Therefore, to explain the broad index distribution observed by Sahraoui et al. (2013) (see also Huang et al. 2014), one needs further analysis of the possible production of high frequencies and their contribution to the frequency spectra measured in the spacecraft frame.

It should also be noted that the anisotropy scaling is $k_z \propto k_{\perp}^{2/3}$ for intermittent low-frequency KAW turbulence formed by the sheet-like fluctuations (Boldyrev & Perez 2012).

The mentioned above problems call for further investigations of the role of intermittency in kinetic Alfvén turbulence.

6.3. Damping effects

In the low-frequency kinetic Alfvén turbulence, possessing parallel electric fields, the proton and electron Landau damping may dissipate the turbulent energy and influence spectral transfer. In this study we neglected these dissipative effects, as well as the ion-cyclotron resonant damping, which needs justifications. To this end we note that even the strongest resonant damping, based on the Maxwellian velocity distributions, does not prevent the super-ion-cyclotron KAWs from propagation. This can be directly seen from Figs. 3-9 by Sahraoui et al. (2012) or Fig. 4 by Vásconez et al. (2014) showing the KAW kinetic dispersion and damping. Even with fixed Maxwellian velocity distributions, many dispersion curves, corresponding to different propagation angles, extend continuously from sub- to super-ion-cyclotron frequencies without being heavily damped. Say, the relative damping rates in Fig. 9 by Sahraoui et al. (2012) are low, $\gamma_L/\omega \lesssim 0.2$, for super-cyclotron KAWs at the propagation angles $> 80^\circ$. Hence the critically balanced turbulent cascade, operating at the wave period time-scale $\gamma_{NL} \simeq \omega$, is still much faster than the dissipation of super-cyclotron KAWs, $\gamma_{NL} \gg \gamma_L$.

Influence of damping on the turbulent spectra can be strong. Cranmer & van Ballegoijen (2003) and Podesta et al. (2010) have shown that the magnetic spectrum of low-frequency kinetic Alfvén turbulence experiences a fast fall-off between ion and electron scales if the Landau damping is accounted for. The frequency spectrum $\propto \omega^{-3.2}$, obtained in numerical simulations by TenBarge & Howes (2012) for $\beta = 1$, is also much steeper than our $\propto \omega^{-2}$ spectrum, which indicates a strong Landau damping in their simulations. Indeed, Podesta et al. (2010) and TenBarge and Howes (2012) used the linear Landau damping ($\gamma_L^{\text{Maxwellian}}$) assuming Maxwellian velocity distributions of plasma species. However, this approximation can hardly be applied to the solar wind where essentially non-Maxwellian particle velocity distributions (PVDs) are regularly observed.

In accordance to recent analytical estimations (Voitenko & De Keyser 2011; Borovsky & Gary 2011; Rudakov et al. 2011; Voitenko & Pierrard 2013) and numerical simulations (Pierrard & Voitenko 2013; Vásconez et al. 2014), the local velocity-space plateaus are formed in the solar wind PVDs by the observed ion-scale turbulence. This conclusion is supported by many in-situ observations of nonthermal features typical for such plateaus. Here we refer to the recent paper by He et al. (2015) demonstrating clear observational evidences of the

quasilinear plateaus rendering $\gamma_L^{\text{Maxwellian}}$ inappropriate. The real damping and its influence on the observed spectra are therefore reduced by the particles feedback (see equation (25) by Voitenko & De Keyser 2011, and following discussions).

To obtain the average spectral index observed in the solar wind (~ -2.8 at $k_{\perp}\rho_i > 1$) from the regular nondissipative spectral index ($\sim -7/3$), one needs to add the index decrement of about -0.47 . In accordance to recent findings, this decrement can be provided by damping (Howes et al. 2011) and/or intermittency (Boldyrev et al. 2012). As the sheet-like intermittency regularly appears in simulations (Boldyrev et al. 2012) and reduces the spectral index to $-8/3$, the rest -0.13 can be attributed to damping. The influence of damping on the turbulent spectra is therefore small, in which case the two-fluid model is a good proxy to study KAW turbulent spectra (see e.g. Boldyrev et al. 2012; Vásconez et al. 2014). Several damping mechanisms can contribute to the -0.13 decrement, including Landau damping, ion-cyclotron damping, non-adiabatic/stochastic heating, etc. (see e.g. Quataert 1998; Voitenko & Goossens 2004; Chandran et al. 2010).

This conclusion is supported by the two-fluid simulations by Boldyrev & Perez (2012) giving the spectral index $\sim -8/3$, similar to the observed indices and to the index ~ -2.8 found in gyrokinetic simulations (Howes et al. 2011b; TenBarge & Howes 2013). This suggests that the dissipative effects are not so important for the turbulent spectra in the solar wind.

When the high-frequency $\omega \sim \omega_{ci}$ KAWs are excited by the turbulent cascade, they can undergo the ion-cyclotron resonance with particles satisfying the resonant condition $\omega - n\omega_{ci} = k_z v_z$ (Hollweg & Isenberg 2002; Voitenko & Goossens 2002, 2003). However, this process depends not solely on the wave frequency, but also on the wave polarization and plasma properties. In particular, both the right-hand polarization of KAWs and the quasilinear modification of the proton velocity distribution reduce the wave damping at the ion-cyclotron resonance. The right-hand polarization allows also a smooth extension of the KAW branch above the ion-cyclotron frequency (Boldyrev et al. 2013). In addition, the ion-cyclotron resonance is narrow-band (see e.g. Fig. 4 by Vásconez et al. 2014), and the turbulent cascade can jump over the narrow resonant layer and proceed further to higher frequencies. These properties of KAWs explain their observations above the ion-cyclotron frequency (Huang et al. 2012).

6.4. Roles of quasilinear premise and critical balance

To model the Alfvénic turbulence we also used a quasilinear premise (e.g., Schekochihin et al. 2009). Its validity has been supported by the gyrokinetic simulations (i.e., Howes et al. 2011b). The quasilinear premise has been widely used to distinguish the wave modes in the dissipation range of the solar wind turbulence (e.g., Sahraoui et al. 2010; He et al. 2011; Salem et al. 2012; Podesta 2013; Roberts et al. 2013, 2015), as well in modeling the kinetic Alfvén turbulence (i.e., Schekochihin et al. 2009; Howes et al. 2011a; Voitenko and De Keyser 2011; Boldyrev & Perez 2012; Zhao et al. 2013). The related assumption of the critical balance between the

linear Alfvén propagation timescale and the nonlinear turnover timescales (Goldreich & Sridhar 1995) is also regularly used in modeling the strong Alfvénic turbulence. Simulations of the kinetic Alfvén turbulence also support this assumption (e.g., Howes et al. 2011b).

Our model assumes local interactions among counter-propagating Alfvénic fluctuations forming the turbulence. Both these assumptions can be violated. The nonlocal spectral transport (Voitenko & Goossens 2005; Zhao et al. 2011a, 2011b, 2014a; Howes et al. 2011b) may contribute to the kinetic-scale spectra and should be taken into account in more comprehensive models. Furthermore, the turbulence generated by the nonlinear interaction between co-propagating waves can produce much steeper spectra. As was shown by Voitenko and De Keyser (2011), the nonlinear interactions among co-propagating KAWs can produce steepest spectra in the vicinity of the ion gyroscale, $P_{\delta b_{\perp}} \propto k_{\perp}^{-3}$ for the strong turbulence and $P_{\delta b_{\perp}} \propto k_{\perp}^{-4}$ for the weak turbulence. It is still unknown which interaction (the interaction between counter-propagating KAWs or the interaction between co-propagating KAWs) or both dominates the kinetic Alfvén turbulence observed in the solar wind.

At last, we note that the universal frequency spectrum of the magnetic power $P_{\delta b_{\perp}}(\omega) \propto \omega^{-2}$ should not surprise the reader. It is a rather natural consequence of the constant energy flux and critical balance conditions and may change only if one or both of the above conditions are violated. For example, if the wave damping becomes strong at very small kinetic scales, the spectral energy flux decreases with k_{\perp} making spectra steeper.

7. SUMMARY

We develop a semi-phenomenological model of Alfvénic turbulence extending from low frequencies $\omega \ll \omega_{ci}$ at MHD scales to high frequencies $\omega \gtrsim \omega_{ci}$ at kinetic scales. The quasi-stationary turbulent spectra are obtained accounting for the dispersive effects of finite $\rho_i k_{\perp}$, $\lambda_e k_{\perp}$, and $\omega/\omega_{ci} \sim \lambda_i k_z$. New findings are summarized as follows:

(1) Generation of high frequencies $\omega/\omega_{ci} \gtrsim 1$ by the turbulent cascade is possible and depends on the injection scale, frequency, and the turbulence state. Larger driving frequency ω_0/ω_{ci} and anisotropy $k_{0z}/k_{0\perp}$ accelerate production of ion-cyclotron frequencies $\omega \sim \omega_{ci}$. Large parallel wavenumbers and frequencies are generated faster in the intermittent turbulence than in the space-filling one, such that intermittent $k_z \propto k_{\perp}^{\alpha/3} k_z$ and

$\tilde{\omega} \propto k_{\perp}^{\alpha/3} \omega$, where $\alpha = 1$ for the sheet-like intermittent structures and $\alpha = 2$ for the tube-like.

(2) Parallel dispersive effects at $\lambda_i k_z \sim \omega/\omega_{ci} > 1$ make kinetic-scale spectra and scalings flatter. In particular, the magnetic spectral index is increased by 1/3 as compared to the low-frequency KAW turbulence. In the space-filling turbulence, $P_{\delta b_{\perp}} \propto k_{\perp}^{-2}$ for $Q \ll \beta \lesssim 1$, and $P_{\delta b_{\perp}} \propto k_{\perp}^{-1}$ for $\beta \ll Q$.

(3) At $\lambda_i k_z \sim \omega/\omega_{ci} \lesssim 1$, the perpendicular dispersive effects of finite $\rho_i k_{\perp}$ (or $\lambda_e k_{\perp}$ at $\beta \ll Q$) dominate and the spectra remain nearly the same as in the low-frequency kinetic Alfvén turbulence, such that $P_{\delta b_{\perp}} \propto k_{\perp}^{-7/3}$ and $P_{\delta e_{\perp}} \propto k_{\perp}^{-1/3}$ in the space-filling turbulence.

(4) Magnetic and electric power spectra are steeper in the intermittent turbulence (\tilde{P}) than in the space-filling (P): $\tilde{P}_{\delta b_{\perp}} \propto k_{\perp}^{-\alpha/3} P_{\delta b_{\perp}}$ and $\tilde{P}_{\delta e_{\perp}} \propto k_{\perp}^{-\alpha/3} P_{\delta e_{\perp}}$. For the mixed sheet- and tube-like intermittency $1 \leq \alpha \leq 2$, which gives the range of possible spectral indices $R_{\text{int}} = [-7/3, -3]$ for $Q \ll \beta \lesssim 1$.

(5) The universal frequency spectrum $E_{\delta b_{\perp}}(\omega) \propto \omega^{-2}$ is found. An apparent contradiction of this universal spectrum with the non-universal effects of intermittency (see item 1 above) can be explained by the dominating cross-field dynamics governing evolution of k_{\perp} , whereas frequency follows k_{\perp} via critical balance. In contrast to $E_{\delta b_{\perp}}(\omega)$, the spectral index of electric frequency spectra $E_{\delta e_{\perp}}(\omega)$ varies with the scale range, turbulence intermittency, and plasma β .

(6) A good correspondence of R_{int} with the range of measured spectral indexes $R_{\text{obs}} = [-2.5, -3.1]$ suggest that the solar wind turbulence at kinetic scale is intermittent and consists of varying fractions of sheet-like and tube-like fluctuations. Shallower spectra may indicate the presence of a fraction of high-frequency fluctuations.

Damping effects are not taken into account in our study, which is justified if the dispersive and intermittency effects are stronger. In the solar wind the turbulent spectral index -2.8 is dominated by the inherent nonlinear dynamics, and only small decrement of the index (about -0.13) can be associated with damping. Weak damping effects can be consequence of the quasilinear and/or nonlinear modifications of the particles velocity distributions, which reduce damping at resonant scales $\rho_i k_{\perp} > 1$.

APPENDIX

WAVE VARIABLES AND SPECTRA IN LOW- β PLASMAS

In low- β ($\beta \ll 1$) plasmas, expressions (2), (4)–(8) can be simplified to

$$\delta b_{\perp} = C_1^{1/2} \epsilon^{1/3} k_{\perp}^{-1/3} \mathcal{R}^{-1/6} \mathcal{L}^{-1/3} \mathcal{L}'^{1/6}, \quad (\text{A1})$$

$$\delta e_{\perp} = C_1^{1/2} \epsilon^{1/3} k_{\perp}^{-1/3} \mathcal{R}^{-2/3} \mathcal{L}^{-1/3} \mathcal{L}'^{-1/3} [(1 + \rho_i^2 k_{\perp}^2) \mathcal{L} - \rho_s^2 k_{\perp}^2 \lambda_i^2 k_z^2], \quad (\text{A2})$$

$$\delta e_z = C_1 C_2 V_A^{-2} \epsilon^{2/3} k_{\perp}^{4/3} \mathcal{R}^{-5/6} \mathcal{L}^{1/3} \mathcal{L}'^{-1/6} [\rho_s^2 (1 + \lambda_i^2 k_z^2) - \lambda_e^2 (1 + \rho_i^2 k_{\perp}^2)], \quad (\text{A3})$$

$$k_z = C_1^{1/2} C_2 V_A^{-1} \epsilon^{1/3} k_{\perp}^{2/3} \mathcal{R}^{-1/6} \mathcal{L}^{2/3} \mathcal{L}'^{1/6}, \quad (\text{A4})$$

$$\omega = C_1^{1/2} C_2 \epsilon^{1/3} k_{\perp}^{2/3} \mathcal{R}^{1/3} \mathcal{L}^{2/3} \mathcal{L}'^{-1/3}, \quad (\text{A5})$$

$$P_{\delta b_{\perp}} = C_1 \epsilon^{2/3} k_{\perp}^{-5/3} \mathcal{R}^{-1/3} \mathcal{L}^{-2/3} \mathcal{L}'^{1/3}, \quad (\text{A6})$$

$$P_{\delta e_{\perp}} = C_1 \epsilon^{2/3} k_{\perp}^{-5/3} \mathcal{R}^{-4/3} \mathcal{L}^{-2/3} \mathcal{L}'^{-2/3} [(1 + \rho_i^2 k_{\perp}^2) \mathcal{L} - \rho_s^2 k_{\perp}^2 \lambda_i^2 k_z^2]^2. \quad (\text{A7})$$

INTERMITTENT TURBULENCE

Alfvénic turbulence is in most cases intermittent (non space-filling), and the turbulent fluctuations occupy only a fraction of volume (see papers by Boldyrev & Perez 2012 and TenBarge & Howes 2013). The probability of intermittent structures in the fluid turbulence is $p(l) \propto l^{3-D}$, where the fractal dimensions are $D = 0, 1$ and 2 for the ball-like, tube-like and sheet-like structures (Frisch 1995). As the Alfvénic turbulent fluctuations are elongated in the direction of mean magnetic field, the isotropic ball-like fluctuations can hardly be developed. For the remaining two structure types we define the probability in the wavenumber space instead of the space of scales: $p(k_{\perp}) = C_p k_{\perp}^{-\alpha}$, where $\alpha = 1$ and 2 for the sheet-like and tube-like structures, respectively. Then, using the energy flux in the intermittent turbulence $\tilde{\epsilon} = p(k_{\perp}) C_1^{-3/2} k_{\perp} \delta \tilde{v}_{e_{\perp}} \delta \tilde{b}_{\perp}^2$, the corresponding wave variables and spectral scalings are found:

$$\delta \tilde{b}_{\perp} = C_p^{-1/3} k_{\perp}^{\alpha/3} \delta b_{\perp}, \quad (\text{B1})$$

$$\delta \tilde{e}_{\perp} = C_p^{-1/3} k_{\perp}^{\alpha/3} \delta e_{\perp}, \quad (\text{B2})$$

$$\delta \tilde{e}_z = C_p^{-2/3} k_{\perp}^{2\alpha/3} \delta e_z, \quad (\text{B3})$$

$$\tilde{k}_z = C_p^{-1/3} k_{\perp}^{\alpha/3} k_z, \quad (\text{B4})$$

$$\tilde{\omega} = C_p^{-1/3} k_{\perp}^{\alpha/3} \omega, \quad (\text{B5})$$

$$\tilde{P}_{\delta b_{\perp}} = C_p^{1/3} k_{\perp}^{-\alpha/3} P_{\delta b_{\perp}}, \quad (\text{B6})$$

$$\tilde{P}_{\delta e_{\perp}} = C_p^{1/3} k_{\perp}^{-\alpha/3} P_{\delta e_{\perp}}. \quad (\text{B7})$$

This work was supported by the Belgian Federal Science Policy Office via Solar-Terrestrial Centre of Excellence (project Fundamental Science) and via IAP Programme (project P7/08 CHARM); by the European Commission via FP7 Program (project 313038 STORM), the NNSFC (11303099, 11373070, 11374262, and 41074107); by the MoSTC (grant 2011CB811402), the NSF of Jiangsu Province (BK2012495), the Key Laboratory of Solar Activity at CAS NAO (LSA201304), the CAEP, and the ITER-CN (2013GB104004).

REFERENCES

- Alexander, D., Harra-Murnion, L. K., Khan, J. I., & Matthews, S. A. 1998, *ApJ*, 494, L235
- Alexandrova, O., Lacombe, C., Mangeney, A., Grappin, R., & Maksimovic, M. 2012, *ApJ*, 760, 121
- Bian, N. H., Kontar, E. P., & Brown, J. C. 2010, *A&A*, 519, A114
- Boldyrev, S., & Perez, J. C. 2012, *ApJ*, 758, L44
- Boldyrev, S., Horaites, K., Xia, Q., & Perez, J. C. 2013, *ApJ*, 777, 41
- Borovsky, J. E., & Gary, S. P. 2011, *JGR*, 116, A07101
- Chandran, B. D. G., Li, B., Rogers, B. N., Quataert, E., & Germaschewski, K. 2010, *ApJ*, 720, 503
- Chaston, C. C., Salem, C., Bonnell, J. W., et al. 2008, *PhRvL*, 100, 175003
- Chaston, C. C., Johnson, J. R., Wilber, M., et al. 2009, *PhRvL*, 102, 015001
- Chen, C. H. K., Sorriso-Valvo, L., Safrankova, J., & Nemecek, Z. 2014, *ApJL*, 789, L8
- Cramer, S. R., & van Ballegoijen, A. A. 2003, *ApJ*, 594, 573
- Frisch, U 1995 *Turbulence: the legacy of A. N. Kolmogorov*
- Gary, G. A. 2001, *SoPh*, 203, 71
- Goldreich, P., & Sridhar, S. 1995, *ApJ*, 438, 763
- He, J., Marsch, E., Tu, C., Yao, S., & Tian, H. 2011, *ApJ*, 731, 85
- He, J., Tu, C., Marsch, E., Bouroaine, S., & Pei, Z. 2013, *ApJ*, 773, 72
- He, J., Wang, L., Tu, C., Marsch, E., Zong, Q. 2015, *ApJL*, 800, L31
- Hollweg, J. V., & Isenberg, P. A. 2002, *JGR*, 107, 1147
- Horbury, T. S., Wicks, R., & Chen, C. H. K. 2012, *SSRv*, 172, 325
- Howes, G. G., TenBarge, J. M., Dorland, W., et al. 2011a *PhRvL*, 107, 035004
- Howes, G. G., TenBarge, J. M., & Dorland, W. 2011b *PhPl*, 18, 102305
- Huang, S. Y., Zhou, M., Sahraoui, F., et al. 2012, *GeoRL*, 39, L11104
- Huang, S. Y., Shraoui, F., Deng, X. H. et al. 2014, *ApJ*, 789, L28
- Kraichnan, R. H. 1965, *PhFl*, 8, 1385
- Podesta, J. J., Borovsky, J. E., & Gary, S. P. 2009, *ApJ*, 712, 685
- Podesta, J. J. 2013, *SoPh*, 286, 529
- Pierrard, V., & Voitenko, Y. 2013, *SoPh*, 288, 355
- Marsch, E. 2006, *Living Rev. Solar Phys.*, 3, 1
- Quataert, E. 1998, *ApJ*, 500, 978
- Quataert, E., & Gruzinov, A. 1999, *ApJ*, 520, 248
- Roberts, O. W., Li, X., & Li, B. 2013, *ApJ*, 769, 58
- Roberts, O. W., Li, X., & Jeska, L. 2015, *ApJ*, 802, 2
- Sahraoui, F., Goldstein, M. L., Belmont, G., Canu, P., & Rezeau, L. 2010, *PhRvL*, 105, 131101
- Sahraoui, F., Belmont, G., Goldstein, M. L. 2012, *ApJ*, 748, 100
- Sahraoui, F., Huang, S. Y., Belmont, G. et al. 2013, *ApJ*, 777, 15
- Salem, C. S., Howes, G. G., Sundkvist, D., et al. 2012, *ApJ*, 745, L9
- Schekochihin, A. A., Cowley, S. C., Dorland, W., et al. 2009, *ApJS*, 182, 310
- TenBarge, J. M., & Howes, G. G. 2012, *PhPl*, 19, 055901
- TenBarge, J. M., & Howes, G. G. 2013, *ApJ*, 771, L27
- Vásconez, C. L., Valentini, F., Camporeale, E., Veltri, P., 2014, *PhPl*, 21, 112107
- Voitenko, Y., & Goossens, M. 2002, *SoPh*, 206, 285
- Voitenko, Y., & Goossens, M. 2003, *SSRv*, 107, 387
- Voitenko, Y., & Goossens, M. 2004, *ApJ*, 605, L149
- Voitenko, Y., & Goossens, M. 2005, *JGR*, 110, A10S01
- Voitenko, Y., & De Keyser, J. 2011, *NPGeo*, 18, 587
- Voitenko, Y., & Pierrard, V. 2013, *Sol. Phys.*, 288, 369
- Wu, P., Perri, S., Osman, K. et al. 2013, *ApJ*, 763, L30
- Zhao, J. S., Wu, D. J., & Lu, J. Y. 2011a, *PhPl*, 18, 032903
- Zhao, J. S., Wu, D. J., & Lu, J. Y. 2011b, *ApJ*, 735, 114
- Zhao, J. S., Wu, D. J., & Lu, J. Y. 2013, *ApJ*, 767, 109
- Zhao, J. S., Voitenko, Y., Wu, D. J., & De Keyser, J. 2014a, *ApJ*, 785, 139
- Zhao, J. S., Voitenko, Y., Yu, M. Y., Lu, J. Y., & Wu, D. J. 2014b, *ApJ*, 793, 107